Size Control of Ti$_4$O$_7$ Nanoparticles by Carbothermal Reduction Using a Multimode Microwave Furnace

Jun Fukushima * and **Hirotsugu Takizawa**

Department of Applied Chemistry, Tohoku University, Aoba Aramaki, Sendai, Miyagi 980-8579, Japan;
takizawa@aim.che.tohoku.ac.jp
* Correspondence: fukushima@aim.che.tohoku.ac.jp; Tel.: +81-22-795-7226

Abstract: Utilization of Ti$_4$O$_7$ in applications such as catalyst support calls for control over the size of the Ti$_4$O$_7$ nanoparticles. This can be achieved using a simple process such as carbothermal reduction. In this study, various sizes of Ti$_4$O$_7$ nanoparticles (25, 60, and 125 nm) were synthesized by carbothermal reduction using a multimode microwave apparatus. It was possible to produce Ti$_4$O$_7$ nanoparticles as small as 25 nm by precisely controlling the temperature, heating process, and holding time of the sample while taking advantage of the characteristics of microwave heating such as rapid and volumetric heating. The results show that microwave carbothermal reduction is advantageous in controlling the size of the Ti$_4$O$_7$ nanoparticles.

Keywords: microwave processing; Ti$_4$O$_7$; nanomaterials; carbothermal reduction; multimode furnace

1. Introduction

Ti$_4$O$_7$ is a Magnéli phase material [1] that exhibits excellent electrical conductivity at room temperature, with a value of about 10^3 S cm^{-1}, which is comparable to graphite [2–4]. In addition, Ti$_4$O$_7$ shows high corrosion resistance [5] and high stability in electrochemical environments [3] as well as acidic electrolytes [6]. From these features, it is possible to use Ti$_4$O$_7$ in different applications, such as unitized regenerative fuel cells [7,8], polymer electrolyte fuel cells [9–11], lithium-sulfur batteries [12–14], and water filtration systems [15,16].

For all these applications, it is necessary to synthesize single-phase Ti$_4$O$_7$ nanomaterials with a high specific surface area [4]. In previous works, Magnéli phase nanoparticles were synthesized using different methods, such as calcination of titanium ethoxide and polyethylene glycol solution [17], thermal plasma treatment of H$_2$TiO$_3$ under Ar/H$_2$ [18], sol-gel and calcination [19], sol–gel and vacuum-carbothermic processes [20], pulsed UV laser irradiation [21], and thermal-induced plasma processes [22]. In addition, Zhang et al. prepared fiber-like Ti$_4$O$_7$ by heating intermediate H$_2$Ti$_3$O$_7$ at 1050 °C under a hydrogen atmosphere [23], but the fibers sintered and became submicron chains. Size control of Ti$_4$O$_7$ nanoparticles is still a challenge because nanoparticles are prone to heavy sintering, e.g., sintering of TiO$_2$ nanoparticles begins at approximately 700 °C [24].

In addition to controlling the size of the nanoparticles, it is also necessary to employ simple, practical techniques for the synthesis. In our previous works, Ti$_4$O$_7$ nanoparticles were prepared using microwave irradiation by a carbothermal reduction process, where the device used was a single-mode furnace [25,26]. To scale up the microwave carbothermal process for industry, the process has to be adapted to multimode furnaces. It is more difficult to control the sample temperature in a multimode-type furnace than in a single-mode microwave furnace because the electromagnetic field distribution tends to be no-uniform in the former case. In order to prepare nanoparticles by the carbothermal reduction process, accurate temperature control is required, especially with rapid temperature increase.

Taking all these factors into account, we synthesized Ti_4O_7 nanoparticles in various sizes (25, 60, and 125 nm) using a carbothermal reduction method with a multimode-type microwave apparatus. Our experimental set-up included a self-made susceptor (using carbon powder with high microwave absorbing power) and proportional–integral–derivative (PID) temperature control.

2. Materials and Methods

Figure 1 shows the sample setting. TiO_2 samples with three particle sizes were used as pristine samples: Sample 1 (TTO-51(A), particle size about 25 nm, Ishihara Sangyo Kaisha, Ltd.), Sample 2 (particle size about 60 nm, 99.5%, IoLiTec-Ionic Liquids Technologies GmbH, Heilbronn, Deutschland), and Sample 3 (particle size about 110 nm, EM Japan Co., Ltd., Tokyo, Japan). Sample 1 was washed with 5M NaOH to eliminate $Al(OH)_3$, which is used as a protective agent. Pristine TiO_2 was dispersed in water with dissolved polyvinylpyrrolidone (PVP, molecular weight: 40,000, Wako Pure Chemical Industries, Ltd., Osaka, Japan) by sonication. The ratio of weight between TiO_2 and PVP is 1.21 g:5.59 g. The solution was dried to obtain PVP-coated TiO_2 nanoparticles. PVP decomposes and becomes a carbon source during microwave heating. The PVP-coated TiO_2 nanoparticles (0.15 g of Sample 1, 0.3 g of Samples 2 and 0.3 g of Sample 3) were filled in a quartz tube. After sealing with silica wool, 0.8 g of titanium sponge (Wako Pure Chemical Industries, Ltd., Osaka, Japan) was added as an oxygen absorber. This quartz tube was set in a quartz container filled with a carbon susceptor. The pressure inside the quartz tube was controlled with a rotary pump so that the base pressure of the system was about 10 Pa. A microwave irradiation furnace from μReactor Ex (Shikoku Instrumentation Co., Ltd., Kagawa, Japan) was used. The process temperature was measured with a thermocouple, which was placed between the susceptor and the quartz tube. Microwave-irradiated samples were analyzed by X-ray diffraction (XRD, RINT-2200/PC, Rigaku Co., Tokyo, Japan) and a field emission scanning electron microscope (FE-SEM, S4800, Hitachi High-Technologies Co., Tokyo, Japan). In the analysis of particle size distribution, we traced each surface of particles in FE-SEM images, and used ImageJ software to calculate the number average particle diameter from the area of traced particles.
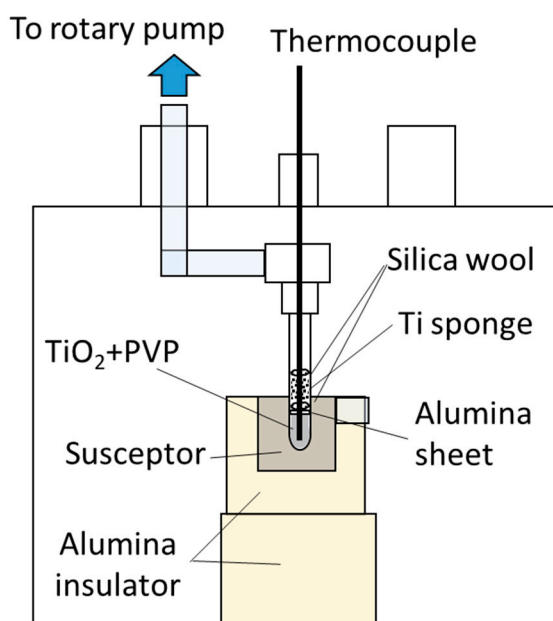
Figure 1. Schematic view of the experimental setup.

3. Results and Discussion

To achieve a reduction of the pristine TiO_2 to Ti_4O_7 and retaining of the nanomorphology of pristineTiO_2 at the same time, various experiments were conducted in different heating regimes to

decide the optimal experiment condition. The experimental results of various heating regime to synthesize Ti_4O_7 nanoparticles from Sample 1 was summarized as Table 1. In 25 nm pristine TiO_2 case, reduction reaction was too fast to obtain Ti_4O_7 when the heating regime was same to the previous paper (No. 7) [25]. To control the reduction-reaction speed in high temperature region, rate of heating, holding temperature and holding time was changed to fast, low and short, respectively. Below 900 °C, sample was not reduced. At 925 °C, Ti_4O_7 phase was obtained, and when the holding time was 13 min, single phase Ti_4O_7 was obtained.

Table 1. Experimental results of various heating regime to synthesize Ti_4O_7 nanoparticles from Sample 1.

No.	Rate of Heating/°C s^{-1}	Holding Temperature/°C	Holding Time/min.	Synthesized Phase
1	12.0	900	10	TiO_2
2	12.0	925	10	$Ti_7O_{13} + Ti_4O_7$
3	12.0	925	11	$Ti_4O_7 + Ti_6O_{11}$
4	12.0	925	13	Ti_4O_7
5	12.0	925	15	$Ti_4O_7 + Ti_3O_5$
6	12.0	925	20	$Ti_3O_5 + Ti_4O_7$
7	10.0	950	30	$Ti_3O_5 + Ti_2O_3$

Figure 2 shows the profiles of microwave power and process temperature during microwave processing when a reduction of the pristine TiO_2 to Ti_4O_7 and retaining of the nanomorphology of pristineTiO_2 was achieved at the same time.
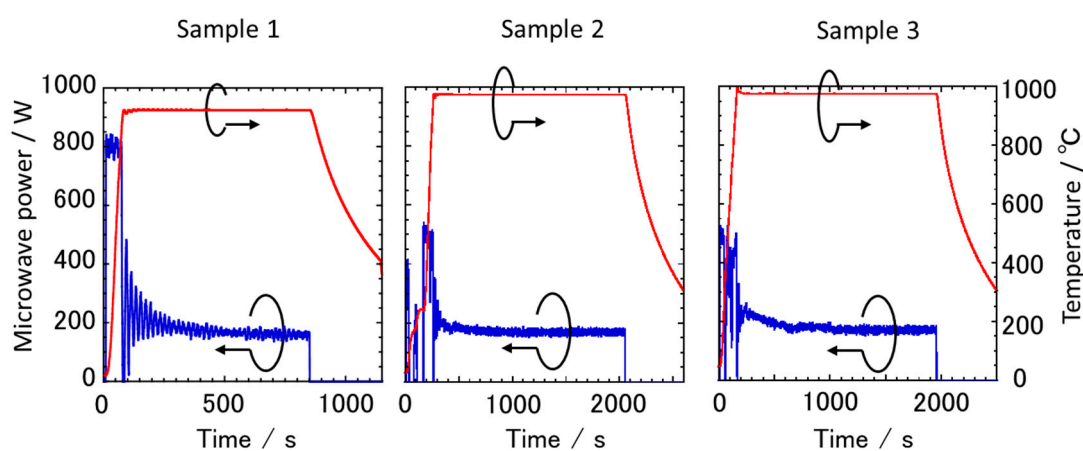
Figure 2. Temperature and microwave power profiles in microwave processing.

Table 2 shows the optimal condition of the rate of heating, holding temperature, holding time, and average microwave power during temperature holding for each process. For Sample 1, the holding temperature was lower and the holding time was shorter than the other samples as a smaller particle size results in a more effective reduction reaction. In addition, to obtain Ti_4O_7 nanoparticles, it is necessary to increase the temperature rapidly and shorten the holding time at high temperatures (above 700 °C) in order to prevent grain growth. The process temperature was 975 °C for Sample 2. This temperature is different compared to a previous study [25] and is due to the temperature measurement method. In the previous study, the thermocouple was located in the sample powder. However, in this experiment, the thermocouple was placed between the susceptor and the quartz tube used to hold the sample powder. Thus, the process temperature measured in this experiment is different from the sample temperature: it is possible that the true sample temperature is lower. We can consider that the temperature of the susceptor is the main factor in maintaining the temperature of the

system because the carbon volume of the susceptor is much larger than that of PVP. Regardless of the particle size, the average microwave power values during the holding process were almost the same.

Table 2. Experimental conditions in microwave processing.

No.	Rate of Heating /$^{\circ}$C s^{-1}	Holding Temperature/$^{\circ}$C	Holding Time/min.	Microwave Power @ Holding/W
Sample 1	12.0	925	13	168.0
Sample 2	3.4	975	30	171.0
Sample 3	5.7	975	30	181.1

Figure 3 shows XRD patterns of pristine TiO_2 and the samples after the microwave process. All pristine TiO_2 samples were in the rutile phase. The right-side figure shows XRD patterns of synthesized samples. In this figure, Ti_4O_7_1, Ti_4O_7_2 and Ti_4O_7_3 refer to synthesized samples after microwave processing from Sample 1, Sample 2 and Sample 3, respectively. The synthesized samples were single-phase Ti_4O_7 without any other Ti-O phase.
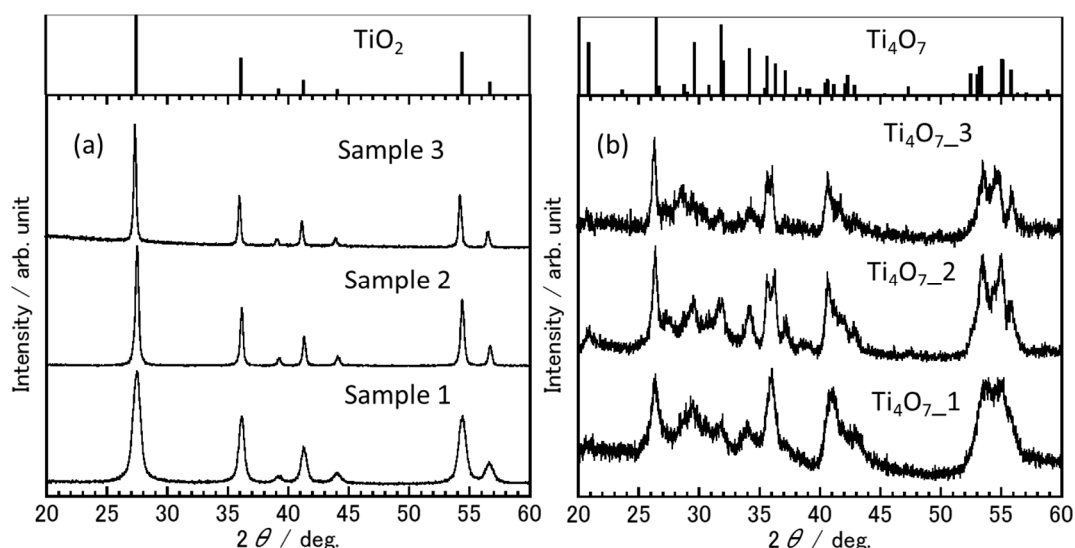
Figure 3. XRD patterns of (**a**) pristine TiO_2 (**b**) the samples after synthesis by microwave process. Ti_4O_7_1, Ti_4O_7_2 and Ti_4O_7_3 refer to particles after synthesis from Sample 1, Sample 2, and Sample 3, respectively.

Crystallite diameters of the pristine TiO_2 and the synthesized Ti_4O_7 were analyzed from XRD patterns using Scherrer equation, and the results were summarized in Table 3. All crystallite diameters were smaller than the primary particle diameter confirmed by FE-SEM: thus the pristine TiO_2 and the synthesized Ti_4O_7 was polycrystalline. The crystallite diameter of pristine TiO_2 was almost the same value as synthesized Ti_4O_7.

Table 3. Crystallite diameter of pristine TiO_2 and synthesized Ti_4O_7 by microwave; MW: microwave.

	Before MW Process	After MW Process
Sample 1	9.2 (0.3) nm	9.2 nm
Sample 2	28.3 (0.4) nm	25.3 nm
Sample 3	31.0 (0.9) nm	29.5 nm

Figure 4 shows FE-SEM images of pristine TiO_2 and synthesized Ti_4O_7 nanoparticles acquired in SE mode. Although some coarse particles were observed in pristine TiO_2, the particle diameter was

uniform. From SE-images of Ti$_4$O$_7$_1 and Ti$_4$O$_7$_2, there seems to be grain growth, but this is because of residual carbon around the Ti$_4$O$_7$ nanoparticles. Figure 5 shows FE-SEM images of the samples acquired in TE mode, where Ti$_4$O$_7$ particles can be clearly observed, since electrons go through the carbon layer. The TE-images for Ti$_4$O$_7$_1 and Ti$_4$O$_7$_2 also show the difference between particles and residual carbon when compared with SE-images. For Ti$_4$O$_7$_3 nanoparticles, the carbon coating was relatively thinner, making it easier to observe and determine the diameter of the nanoparticles.
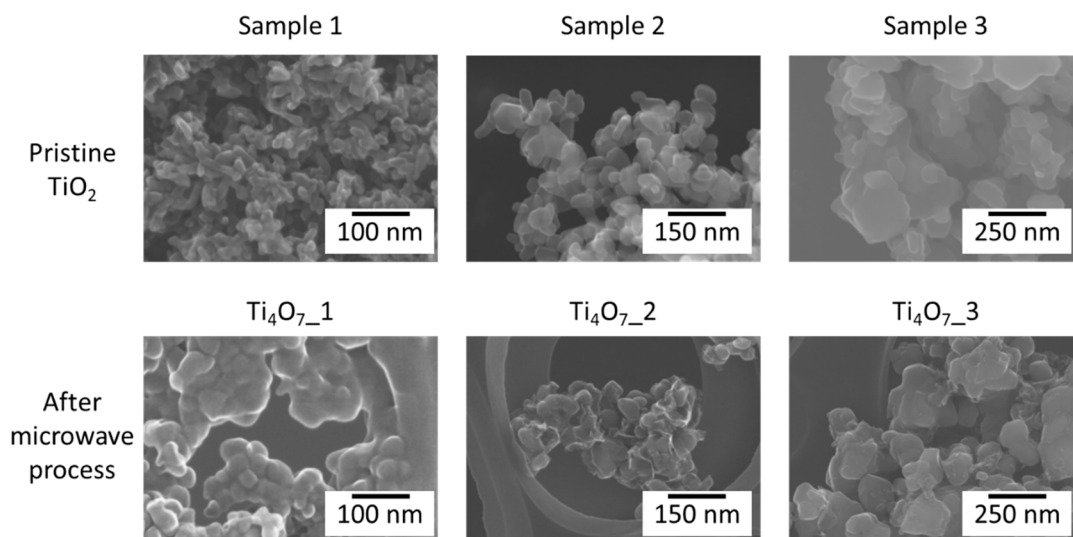
Figure 4. FE-SEM (field emission scanning electron microscope) images of pristine TiO$_2$ and synthesized Ti$_4$O$_7$ nanoparticles acquired in secondary electron (SE) mode.
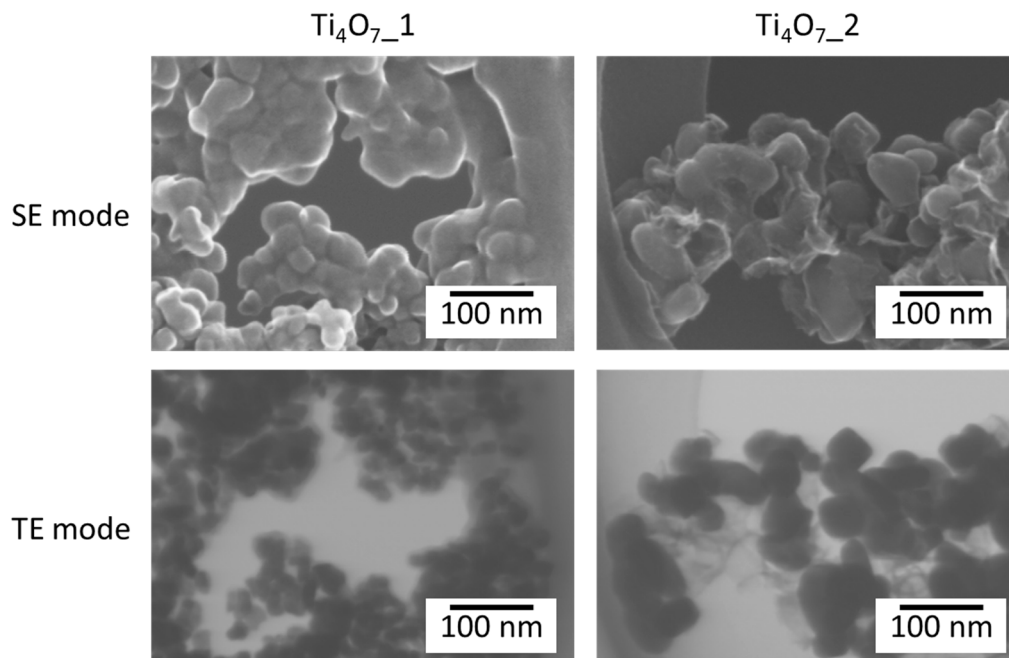
Figure 5. FE-SEM images of Ti$_4$O$_7$_1 and Ti$_4$O$_7$_2 acquired in SE and transmission electron (TE) mode.

Figure 6 shows histograms of particle sizes for pristine TiO$_2$ and synthesized Ti$_4$O$_7$. Table 4 shows the average particle size (Ave. diameter), standard deviation (S.D.), maximum particle diameter (Max.), minimum particle diameter (Min.), sample number (n), and standard error (S.E.). The average nanoparticle diameter of Sample 1, Sample 2, and Sample 3 was 25.8, 54.6, and 108.0 nm, respectively. The average nanoparticle diameter of Ti$_4$O$_7$_1 was 24.7 nm, which is within the error margin of the

average diameter of Sample 1. On the other hand, the average nanoparticle diameter of $Ti_4O_7\_2$ was 60.4 nm; indicating a 3.3 nm grain growth. For $Ti_4O_7\_3$, the average nanoparticle diameter was 6.3 nm larger compared to the average nanoparticle diameter of Sample 3. However, since the maximum particle size of Sample 3 was larger than the measured sizes of $Ti_4O_7\_3$ particles, it can be deduced that there was no significant grain growth.
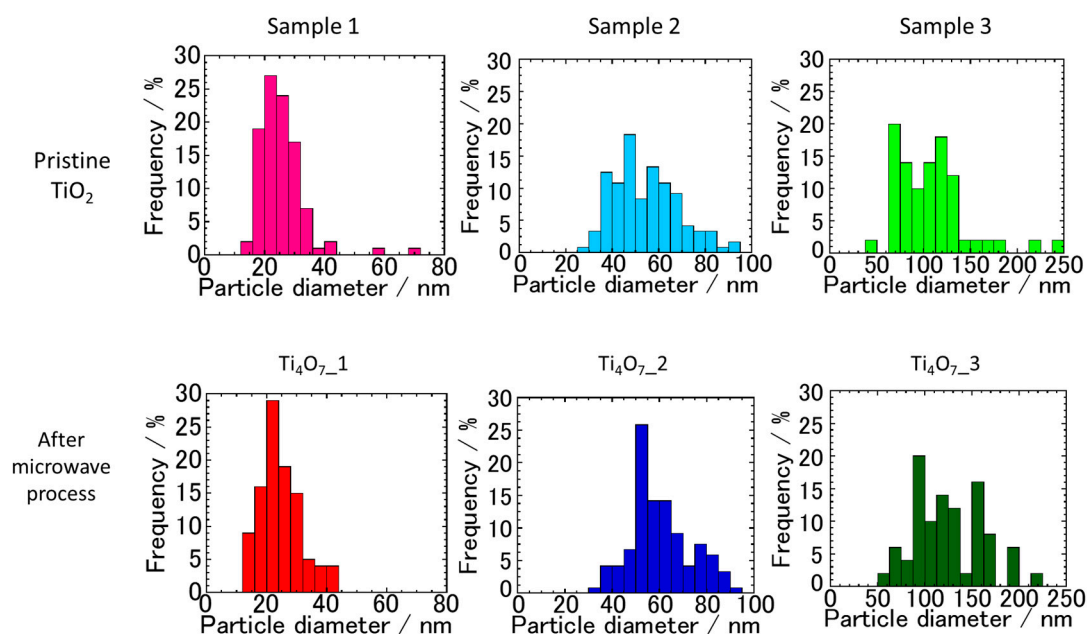
Figure 6. Histograms of nanoparticle size of pristine and synthesized Ti_4O_7.

Table 4. Average particle size (Ave. diameter), standard deviation (S.D.), maximum particle diameter (Max.), minimum particle diameter (Min.), sample number (n), and standard error (S.E.) of pristine TiO_2 and synthesized Ti_4O_7.

No.	Ave. Diameter/nm	S.D./nm	Max./nm	Min./nm	*n*/-	S.E./nm
Sample 1	25.8	7.9	69.5	13.9	100	0.8
$Ti_4O_7\_1$	24.7	6.7	43.5	12.2	100	0.7
Sample 2	54.6	13.9	91.1	29.2	120	1.3
$Ti_4O_7\_2$	60.4	12.8	94.6	30.7	120	1.2
Sample 3	108.0	38.0	246.2	41.8	50	5.4
$Ti_4O_7\_3$	125.0	37.5	215.6	51.0	50	5.3

From these results, even when a simple apparatus such as a multimode microwave irradiation furnace is used, it is possible to produce Ti_4O_7 nanoparticles with an average size as low as 25 nm. This can be done using a carbon thermal reduction method by precise control of the heating rate, holding temperature, and holding time.

4. Conclusions

Ti_4O_7 nanoparticles of various sizes (25, 60, 125 nm) were prepared in a multimode microwave furnace. In general, the synthesized Ti_4O_7 nanoparticles retained the size of the pristine TiO_2 nanoparticles. The process time and temperature varied depending on the size of nanoparticles because the reduction reaction was slower when larger pristine nanoparticles were used. It is possible to precisely control the temperature, heating process, and holding time of the sample while taking advantage of the characteristics of microwave heating such as rapid and volume heating. This microwave carbothermal reduction method is thus highly effective in controlling the size of the synthesized Ti_4O_7 particles.

References

1. Andersson, S.; Collén, B.; Kuylenstierna, U.; Magnéli, A. Phase Analysis Studies on the Titanium-Oxygen System. *Acta Chem. Scand.* **1957**, *11*, 1641–1652. [CrossRef]

2. Bartholomew, R.F.; Frankl, D.R. Electrical properties of some titanium oxides. *Phys. Rev.* **1969**, *187*, 828–833. [CrossRef]

3. Smith, J.R.; Walsh, F.C. Electrodes based on Magneli phase titanium oxides: The properties and applications of Ebonex materials. *J. Appl. Electrochem.* **1998**, *28*, 1021–1033. [CrossRef]

4. Walsh, F.C.; Wills, R.G.A. The continuing development of Magnéli phase titanium sub-oxides and Ebonex®electrodes. *Electrochim. Acta* **2010**, *55*, 6342–6351. [CrossRef]

5. Ioroi, T.; Senoh, H.; Yamazaki, S.I.; Siroma, Z.; Fujiwara, N.; Yasuda, K. Stability of Corrosion-Resistant Magnéli-Phase Ti_4O_7-Supported PEMFC Catalysts at High Potentials. *J. Electrochem. Soc.* **2008**, *155*, B321. [CrossRef]

6. Graves, J.E.; Pletcher, D.; Clarke, R.L.; Walsh, F.C. The electrochemistry of Magnéli phase titanium oxide ceramic electrodes Part I. The deposition and properties of metal coatings. *J. Appl. Electrochem.* **1991**, *21*, 848–857. [CrossRef]

7. Chen, G.; Bare, S.R.; Mallouk, T.E. Development of Supported Bifunctional Electrocatalysts for Unitized Regenerative Fuel Cells. *J. Electrochem. Soc.* **2002**, *149*, A1092. [CrossRef]

8. Won, J.; Kwak, D.; Han, S.; Park, H.; Park, J.; Ma, K.; Kim, D.; Park, K. $PtIr/Ti_4O_7$ as a bifunctional electrocatalyst for improved oxygen reduction and oxygen evolution reactions. *J. Catal.* **2018**, *358*, 287–294. [CrossRef]

9. Ota, K.; Matsuzawa, K.; Nagai, T.; Ishihara, A.; Mitsushima, S. Stability of Group 4 and 5 Metal Oxide Cathode with Titanium Oxide Support for PEFCs. *Meet. Abstr.* **2016**, *MA2016-01*, 1713.

10. Ioroi, T.; Senoh, H.; Siroma, Z.; Yamazaki, S.; Fujiwara, N.; Yasuda, K. Stability of Corrosion-Resistant Magnéli-Phase Ti_4O_7-Supported PEMFC Catalysts. *ECS Trans.* **2007**, *11*, 1041–1048.

11. Ioroi, T.; Akita, T.; Yamazaki, S.; Siroma, Z.; Fujiwara, N.; Yasuda, K. Corrosion-Resistant PEMFC Cathode Catalysts Based on a Magnéli-Phase Titanium Oxide Support Synthesized by Pulsed UV Laser Irradiation. *J. Electrochem. Soc.* **2011**, *158*, C329. [CrossRef]

12. Mei, S.; Jafta, C.J.; Lauermann, I.; Ran, Q.; Kärgell, M.; Ballauff, M.; Lu, Y. Porous Ti_4O_7 Particles with Interconnected-Pore Structure as a High-Efficiency Polysulfide Mediator for Lithium–Sulfur Batteries. *Adv. Funct. Mater.* **2017**, *27*, 1–10. [CrossRef]

13. Wei, H.; Rodriguez, E.F.; Best, A.S.; Hollenkamp, A.F.; Chen, D.; Caruso, R.A. Chemical Bonding and Physical Trapping of Sulfur in Mesoporous Magnéli Ti_4O_7 Microspheres for High-Performance Li–S Battery. *Adv. Energy Mater.* **2017**, *7*, 1601616. [CrossRef]

14. Zhang, Y.; Yao, S.; Zhuang, R.; Luan, K.; Qian, X.; Xiang, J.; Shen, X.; Li, T.; Xiao, K.; Qin, S. Shape-controlled synthesis of Ti_4O_7 nanostructures under solvothermal-assisted heat treatment and its application in lithium-sulfur batteries. *J. Alloys Compd.* **2017**, *729*, 1136–1144. [CrossRef]

15. Santos, M.C.; Elabd, Y.A.; Jing, Y.; Chaplin, B.P.; Fang, L. Highly Porous Ti_4O_7 Reactive Electrochemical Water Filtration Membranes Fabricated via Electrospinning/Electrospraying. *AIChE J.* **2016**, *62*, 508–524. [CrossRef]

16. Guo, L.; Jing, Y.; Chaplin, B.P. Development and Characterization of Ultrafiltration TiO2 Magnéli Phase Reactive Electrochemical Membranes. *Environ. Sci. Technol.* **2016**, *50*, 1428–1436. [CrossRef] [PubMed]

17. Pang, Q.; Kundu, D.; Cuisinier, M.; Nazar, L.F. Surface-enhanced redox chemistry of polysulphides on a metallic and polar host for lithium-sulphur batteries. *Nat. Commun.* **2014**, *5*, 4759. [CrossRef] [PubMed]

18. Xu, B.; Zhao, D.; Sohn, H.Y.; Mohassab, Y.; Yang, B.; Lan, Y.; Yang, J. Flash synthesis of Magnéli phase (Ti_nO_{2n-1}) nanoparticles by thermal plasma treatment of H2TiO3. *Ceram. Int.* **2018**, *44*, 3929–3936. [CrossRef]

19. Portehault, D.; Maneeratana, V.; Candolfi, C.; Oeschler, N.; Veremchuk, I.; Grin, Y.; Sanchez, C.; Antonietti, M. Facile general route toward tunable magnéli nanostructures and their use as thermoelectric metal oxide/carbon nanocomposites. *ACS Nano* **2011**, *5*, 9052–9061. [CrossRef] [PubMed]

20. Huang, S.S.; Lin, Y.H.; Chuang, W.; Shao, P.S.; Chuang, C.H.; Lee, J.F.; Lu, M.L.; Weng, Y.T.; Wu, N.L. Synthesis of High-Performance Titanium Sub-Oxides for Electrochemical Applications Using Combination of Sol-Gel and Vacuum-Carbothermic Processes. *ACS Sustain. Chem. Eng.* **2018**, *6*, 3162–3168. [CrossRef]

21. Ioroi, T.; Kageyama, H.; Akita, T.; Yasuda, K. Formation of electro-conductive titanium oxide fine particles by pulsed UV laser irradiation. *Phys. Chem. Chem. Phys.* **2010**, *12*, 7529. [CrossRef] [PubMed]

22. Arif, A.F.; Balgis, R.; Ogi, T.; Iskandar, F.; Kinoshita, A.; Nakamura, K.; Okuyama, K. Highly conductive nano-sized Magnéli phases titanium oxide (TiOx). *Sci. Rep.* **2017**, *7*, 3646. [CrossRef] [PubMed]

23. Han, W.Q.; Zhang, Y. Magnéli phases Ti_nO_{2n-1} nanowires: Formation, optical, and transport properties. *Appl. Phys. Lett.* **2008**, *92*, 203117. [CrossRef]

24. Toyoda, M.; Yano, T.; Tryba, B.; Mozia, S.; Tsumura, T.; Inagaki, M. Preparation of carbon-coated Magneli phases Ti_nO_{2n-1} and their photocatalytic activity under visible light. *Appl. Catal. B Environ.* **2009**, *88*, 160–164. [CrossRef]

25. Takeuchi, T.; Fukushima, J.; Hayashi, Y.; Takizawa, H. Synthesis of Ti_4O_7 Nanoparticles by Carbothermal Reduction Using Microwave Rapid Heating. *Catalysts* **2017**, *7*, 65. [CrossRef]

26. Fukushima, J.; Takeuchi, T.; Hayashi, Y.; Takizawa, H. Microwave synthesis of carbon-coated Ti_4O_7 nanorods by rapid carbothermal reduction processing. *Chem. Eng. Process. Process Intensif.* **2018**, *125*, 27–33. [CrossRef]